The 1997 Fluids Engineering Division Summer Meeting
FEDSM'97
June 22-26, 1997

FEDSM97-3563

EXPERIMENTAL SIMULATION OF A BOW WAVE

TRICIA A. WANIEWSKI, CHRISTOPHER E. BRENNEN, AND FREDERIC RAICHLEN
DIVISION OF ENGINEERING AND APPLIED SCIENCE
CALIFORNIA INSTITUTE OF TECHNOLOGY
PASADENA, CALIFORNIA 91125
TEL:(818)395-4147, FAX: (818)568-2719, EMAIL: WANIEWSK@PLESSET.CALTECH.EDU

ABSTRACT

In flows around ships, the bow wave can entrain a significant amount of air as it breaks continuously on the free surface. The resulting air bubbles persist in the ship wake affecting its radar cross section as well as acting as cavitation nuclei in the flow entering the ship's propeller. In the present investigation, the formation of a bow wave on a ship was simulated in the laboratory using a deflecting plate in a supercritical free surface flow. The experiments were conducted at two scales. The present paper focuses on how the bow wave changes with the angles and flow parameters, information which is a necessary prerequisite for understanding the air entrainment process. Flow visualization studies were performed and an electronic point gage was used to study the three-dimensional shape of the bow waves and the manner in which they break.

NOMENCLATURE

d	Depth (m)
$\mathbf{F}$	Froude number based on depth, $\mathbf{F} = U/\sqrt{gd}$
g	Gravitational acceleration (m/s^2)
Q	Flow rate (m^3/s)
r	Horizontal coordinate along the deflecting plate
r'	Non-dimensional coordinate along the deflecting plate, $r' = r/\mathbf{F}d$
U	Free stream velocity (m/s)
x	Streamwise coordinate
x'	Non-dimensional streamwise coordinate, $x' = x/\mathbf{F}d$
y	Cross stream coordinate
y'	Non-dimensional cross stream coordinate, $y' = y/\mathbf{F}d$
z	Vertical coordinate
Z	Free surface height
Z'	Non-dimensional free surface height, $Z' = 90Z/\mathbf{F}d\theta$
Z''	Non-dimensional free surface height, $Z'' = Z/\mathbf{F}d$
ϕ	Dihedral angle (degrees)
θ	Wedge half angle (degrees)

INTRODUCTION

Air entrainment by breaking waves is important not only from an engineering standpoint but also from an environmental standpoint. As a result, there have been numerous experimental studies measuring bubble size distributions from breaking waves in the laboratory as well as in the field. Researchers have simulated steady breaking waves in the laboratory by towing a submerged hydrofoil (Duncan, 1981), towing a wedge (Ogilvie, 1969 and Miyata, 1984), producing a continuous waterfall (Cipriano and Blanchard, 1981), and by producing a simple plunging jet (Chanson and Cummings, 1994 and Bonetto and Lahey, 1992). Lamarre and Melville [1991] showed that the breaking wave dynamics are closely coupled with the air entrainment process. Loewen et al.

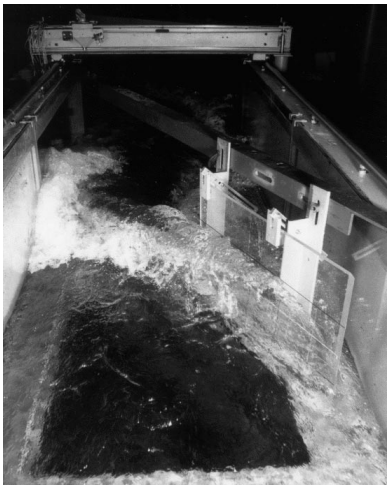

FIGURE 1: Photograph of the test section looking downstream from above; $\theta = 13.4°$, $\phi \approx 15°$, $U = 2.45m/s$, $d = 11.45cm$, and $\mathbf{F} = 2.31$.

[1996] summarize the experimental studies and present results on size distributions for large bubbles produced by mechanically generated breaking waves. Virtually all of these investigations focus on "two-dimensional" wave breaking and there is little information on the highly three-dimensional processes which occur in a breaking bow wave.

The present investigation of a simulated bow wave is a part of a program to examine the air entrainment by breaking bow waves. It uses a stationary deflecting plate in a supercritical free surface flow to simulate a breaking bow wave, to more closely examine the breaking process.

EXPERIMENTAL APPARATUS

Experiments were conducted at two different scales. The larger scale experiments were conducted in a 40 m long tilting flume with a slope of 1:50. The flume is 1.1 m wide and 0.61 m deep with glass sidewalls and a stainless steel bottom. Flow rate, Q, is measured using a venturi meter and the depth, d, is measured with a point gage. The maximum discharge is approximately $0.394m^3/sec$ [Vanoni et al., 1967]. To create a super-critical flow, a two-dimensional spillway section was installed at the upstream end of the flume. It also provided a settling region for the inflow which dissipates, to some extent, the larger scale turbulence which occurs at the flume inlet. In addition, several flow-smoothing devices were installed upstream of the spillway.

The test section is located approximately 24 m, or over 200 depths, downstream of the spillway. This ensures a fully developed flow and also gives the air bubbles entrained in the flow downstream of the deflecting plate a long time to settle out. The test section has an 80.0 cm wide, 121 cm long, and 2.5 cm thick glass window installed in the stainless steel bottom. Above this window, a 76 cm long by 50 cm high lucite plate was mounted at an angle θ to the oncoming flow to simulate a wedge shaped hull with half angle θ and dihedral angle ϕ. Its leading edge was machined to a sharp edge and displaced a few cm from the glass flume sidewall to eliminate wall boundary layer effects on the flow on the plate. A steady breaking wave, similar to that observed at the bow of a ship, is created as the flow rides up on the plate as shown in Figure 1. The flow could also be observed from below through the glass window using a mirror supported at an angle of 45° beneath the flume.

The free surface height is measured using an electronic point gage. The percentage of time that the point is immersed can be preset, and a servo motor system connected to the point gage maintains this immersion percentage. The gage produces an electrical signal which is, through calibration, proportional to the water surface elevation. It is attached to a carriage, visible in Figure 1, which travels on precision rails mounted to the top of the flume sidewalls. The electronic point gage can be moved in the cross-stream and downstream directions by two servo motors. A PC controls these servo motors so that the electronic point gage can automatically traverse a 20 by 20 point grid in the bow wave region.

Smaller scale experiments were conducted in a recirculating glass bottom tilting flume 265 cm long, 45.9 cm wide, and 12.7 cm deep using a lucite deflector plate 13 cm high and 45 cm long. The flow was adjusted using either a flow control valve downstream of the pump or a flap nozzle located at the entrance to the channel. An orifice meter with a mercury/water manometer was used to determine the flow rate (maximum about $0.01m^3/s$). The electronic point gage was positioned manually and used to measure the free surface height.

FLOW VISUALIZATION

Flow visualization studies were performed to define the main features of the flow, especially those visible through the glass window in the bottom of the flume. Figure 2 shows an exaggerated schematic of this view with the key features labeled. Syringes with cannulae were used to inject kriegrocine red and blue dye into the flow and the flow was recorded using a video camera, high speed movie camera, and a Nikon N90AF still camera.

In Figure 2, the planform profile of the wave jet,

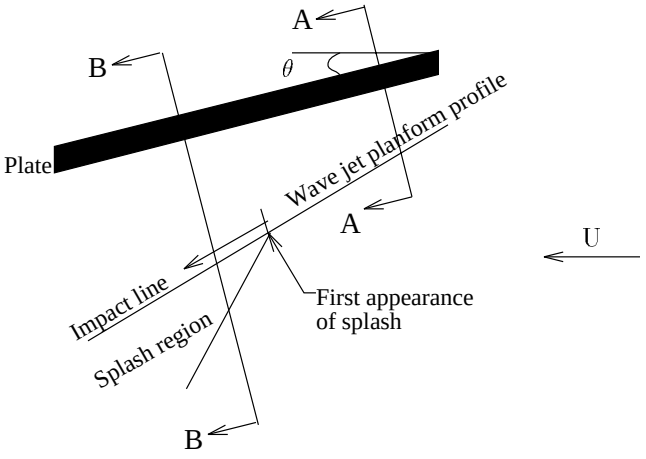

FIGURE 2: Schematic diagram of the flow features.

the impact line, and the splash region are indicated. These features are clarified in the cross-sectional views presented in Figure 3. The impingement of the flow on the deflecting plate creates a liquid sheet which rides up on the plate. The maximum height of the breaking wave is located a few cm off of the deflecting plate and a thin secondary liquid sheet is observed in the larger scale experiments as in Figure 3.

Once the wave has reached its maximum height, it begins to plunge back towards the free surface as shown in cross-section B in Figure 3. Inspection of the breaking wave jet reveals almost equally spaced striations along the surface oriented perpendicular to the deflector plate. The edge of the breaking wave is very rough and appears almost to be comprised of individual jets as can be seen in Figure 4. It impacts along a line called the impact line in Figure 2.

Photographs show that entrained air is visible beneath the free surface as bubble clouds which are convected downstream by the flow. These bubble clouds seem to grow in size at a steady rate until they encounter the bottom of the flume and/or the opposite wall. A typical photograph of such clouds is presented in Figure 5. It is suspected that the periodicity of the bubble clouds is related to the periodicity of the observed surface irregularities in the breaking wave as shown in Figure 4.

After the wave jet impacts the free surface, a splash region is formed as seen in Figures 1 and 4 and shown schematically in Figures 2 and 3. Although the majority of the splash is formed by the wave jet "bouncing" off the undisturbed free surface, the flow visualization tests with dye showed that some of the upstream flow at the free surface is deflected and also enters the splash region. The splash region has a limited upstream extent

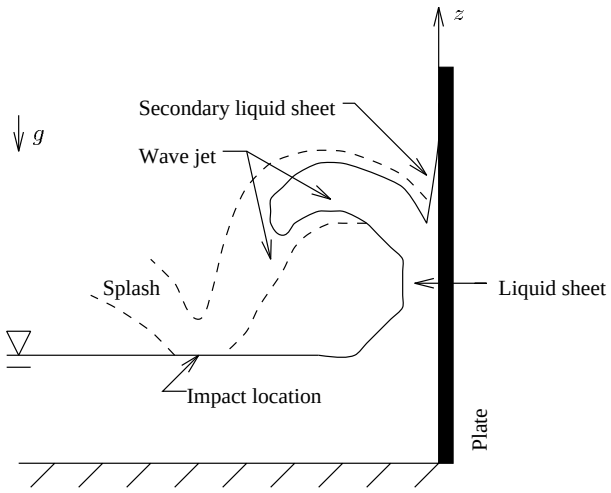

FIGURE 3: Cross-sectional views A (solid line) and B (dashed line) from figure 2 of the flow features. The horizontal coordinate along the plate, r, is perpendicular to the plane of the paper.

as sketched in Figure 2.

EXPERIMENTAL RESULTS

The electronic point gage was used to measure the three dimensional shape of the bow wave for different angles and flow parameters. Wave profiles for three different Froude numbers, approximately: $\mathbf{F} = 2.6$, $\mathbf{F} = 2.8$, and $\mathbf{F} = 3.1$ were studied for deflection angles, $\theta = 13.4°$ and $26.6°$ and zero dihedral angle, ϕ. In the larger scale experiments two grids were traversed over a period of four hours while the flow rate, velocity, and depth were closely monitored. At each grid point traversed by the electronic point gage, an average of 40 elevation readings was obtained over a period of approximately 2 sec. At the conclusion of the experiments, the two grids were averaged to produce a water surface topography. Figure 6 shows the orientation of the coordinate system with the leading edge of the deflecting plate as the origin along with the orientation of the region sampled for the surface topography.

After the grids were completed, the profile of the bow wave along the deflecting plate, defined herein as the contact line, was measured by moving the electronic point gage manually and averaging out the unsteadiness in the vertical direction for a set immersion percentage. These results were non-dimensionalized as in Ogilvie [1969]. The geometric mean of d and U^2/g, $\mathbf{F}d$, was used to non-dimensionalize the distance along the plate i.e., $r' = r/\mathbf{F}d$. The product of this factor and

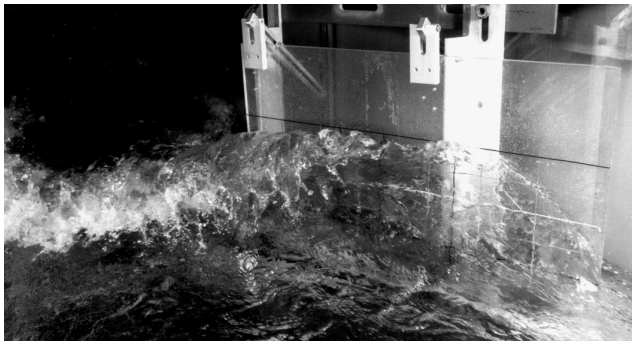

FIGURE 4: A photograph of the simulated bow wave; $\theta \approx 26°$, $\phi \approx 15°$, $U = 2.45m/s$, $d = 11.45cm$, and $\mathbf{F} = 2.31$.

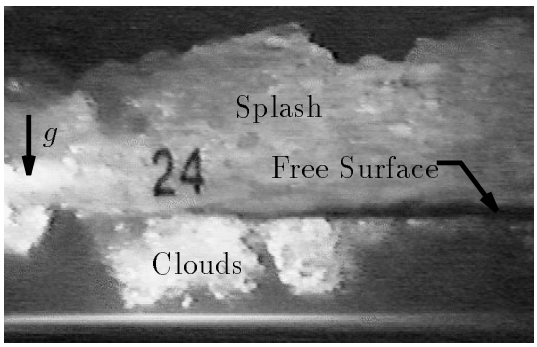

FIGURE 5: A photograph looking beneath the free surface at the periodic bubble clouds; $\theta \approx 26°$, $\phi \approx 15°$, and the flow is from right to left.

$180/2\theta$ was used to non-dimensionalize the free surface height i.e., $Z' = 90Z/\mathbf{F}d\theta$.

Finally, for the larger scale experiments, cross sections of the plunging wave jet similar to that shown by the dashed line in Figure 3 were measured using the electronic point gage. The electronic point gage was positioned manually and a special tip was used to measure the underside of the wave jet; however, it was not possible to resolve this surface completely because of the splash.

WAVE PROFILE AND JET CROSS SECTION RESULTS

Figure 7 presents the non-dimensional profiles of the bow wave on the deflecting plate from the smaller scale experiments. The profiles for both angles for $2.57 < \mathbf{F} < 3.06$ are similar, although the amplitude of the profile for $\theta = 26.3°$ is slightly greater than that for $\theta = 13.2°$. It also appears that for a particular angle θ, the amplitude increases with $\mathbf{F}$. The slight rise in most

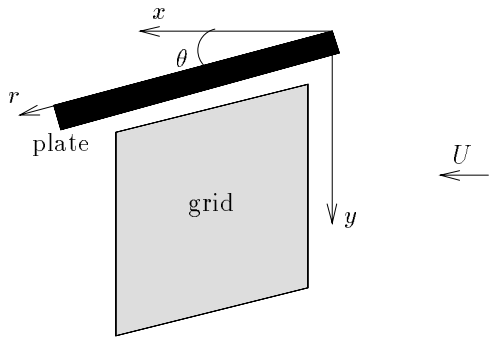

FIGURE 6: Cross sectional view of the deflecting plate and the electronic point gage sampling grid looking down from above. The vertical coordinate, z, is perpendicular to the plane of the paper.

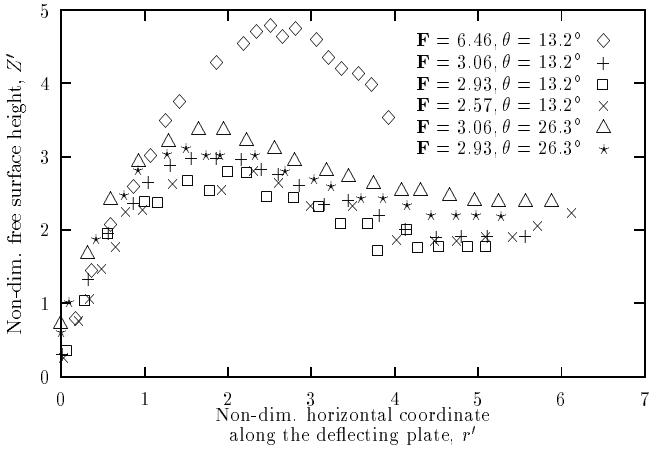

FIGURE 7: Non-dimensional profiles of the bow wave along the deflecting plate from smaller scale experiments with two different angles θ.

of the profiles occurring at $r' \approx 5$ is caused by end effects associated with the deflecting plate. For $\theta = 13.2°$ and $\mathbf{F} = 6.46$ the data are quite different than for smaller $\mathbf{F}$. The data were also non-dimensionalized using d and U^2/g, but neither factor improved the agreement of the profiles. This difference in the profiles may be due to nonlinear effects. This speculation is supported by the observation that the curves agree reasonably well near the leading edge of the plate, where nonlinearities are probably small.

The non-dimensional profiles of the bow wave along the deflecting plate for the larger scale experiments are presented in Figure 8. The profiles for the two angles, $\theta = 13.4°$ and $\theta = 26.6°$, are quite different; the profiles

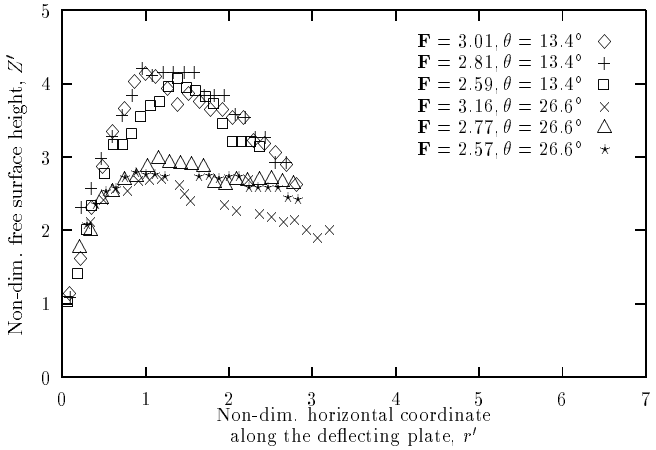

FIGURE 8: Non-dimensional profiles of the bow wave along the deflecting plate from larger scale experiments with two different angles θ.

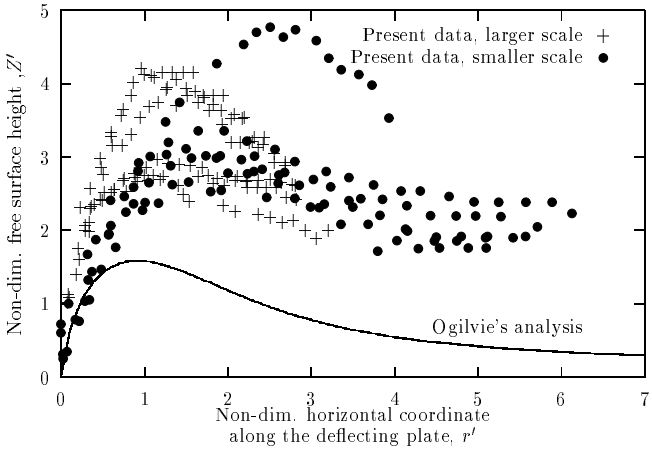

FIGURE 9: Comparison of the non-dimensional profiles of the bow wave along the deflecting plate from the smaller scale and the larger scale experiments. Ogilvie's analytical profile is shown as a solid black line.

for $\theta = 26.6°$ have a greater amplitude than the profiles for $\theta = 13.4°$. However, even after the data were non-dimensionalized the amplitudes were still quite different. This suggests that the bow wave profiles do not simply scale linearly with angle θ as suggested by Ogilvie [1969] and that there apparently is a more complicated relationship.

The non-dimensional profiles of the bow wave for the larger and smaller scale experiments are compared in Figure 9. In general, the profiles agree near the leading edge of the plate but deviate significantly thereafter. Also in Figure 9, these profiles are compared to the contact line obtained analytically by Ogilvie [1969] for the bow region of a finite draft slender body moving in an infinitely deep ocean. The analytical profile is the same for all values of $\mathbf{F}$. Clearly these experiments showed poor agreement with his analysis. Ogilvie also conducted towed wedge experiments which also showed poor agreement with his analysis. He attributed the discrepancy to the limitation of his thin wedge approximation.

In Ogilvie's experiments, the maximum value of Z' was shown to vary with $\mathbf{F}$ and θ. Figure 10 shows his results for $\theta = 15°$ and four different values of d. Also shown is Z'_{max} for the smaller and larger scale experiments of this study for $\theta = 13.4°$ and for the different Froude numbers. The smaller scale experiments agree with Ogilvie's results even though d was much smaller. This suggests that depth does not have a large effect on the bow wave profiles, even for such a small scale experiments where surface tension effects might be expected. More importantly, it shows that similar results can be produced by experiments using either a towed wedge of limited draft in a large depth or by using a deflector plate extending the full depth in a steady stream. The larger scale experiments show a greater deviation possibly due to the presence of a thin secondary liquid sheet on the deflecting plate which was shown schematically in Figure 3. The electronic point gage measured the location of the top of this secondary sheet for the larger scale experiments and where applicable this was plotted in Figure 8, but it was not observed in the smaller scale experiments. Furthermore, since Ogilvie determined Z'_{max} using photographs it is likely that a secondary sheet was not observed in his experiments either.

Figure 11 presents some typical non-dimensional cross sections of the plunging wave jet from the larger scale experiments. For each flow condition, cross sections were measured for three different streamwise locations. Using these cross sections, the jet thickness and the angle of impingement were measured. For each Froude number tested at $\theta = 25.4°$, the jet was on the order of 5 cm thick and the angle of impingement was approximately 30°.

WATER SURFACE TOPOGRAPHY RESULTS

An example of a water surface topography from the larger scale experiments for $\theta = 13.4°$ is shown in Figure 12. The figure depicts the three-dimensional water surface profile for the sampling region indicated in Figure 6, and all data were non-dimensionalized using the factor $\mathbf{F}d$. The sampling region for this topography was located upstream of the splash region and so it only includes the initial stages of the formation of the breaking

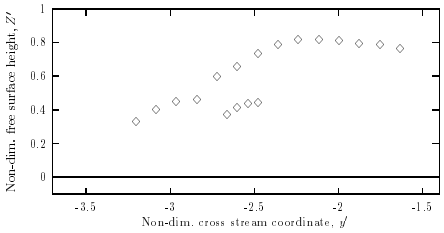

(a) Jet cross-section at non-dim. streamwise coordinate, $x' = 3.46$

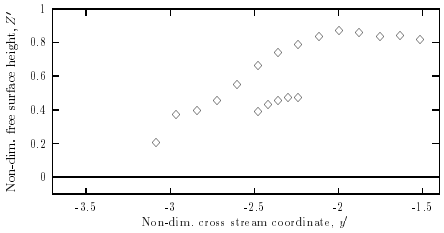

(b) Jet cross-section at non-dim. streamwise coordinate, $x' = 3.21$

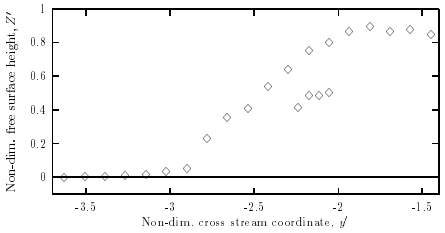

(c) Jet cross-section at non-dim. streamwise coordinate, $x' = 2.96$

FIGURE 11: Non-dimensional experimental cross-sections of the plunging wave jet for different distances downstream of the deflecting plate leading edge; $\theta = 25.4°$, $U = 2.41m/s$, $d = 6.72cm$, and $\mathbf{F} = 2.97$. The undisturbed free surface is $Z' = 0$ and the leading edge of the plate is at $(x', y') = (0, 0)$.

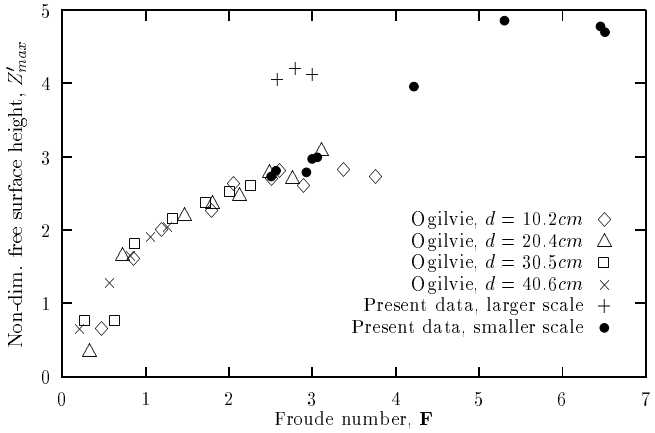

FIGURE 10: Comparison of the $\theta = 13.4°$ smaller scale ($d = 1.4cm$) and larger scale ($d \approx 7.8cm$) experimental results to Ogilvie's $\theta = 15°$ experimental results.

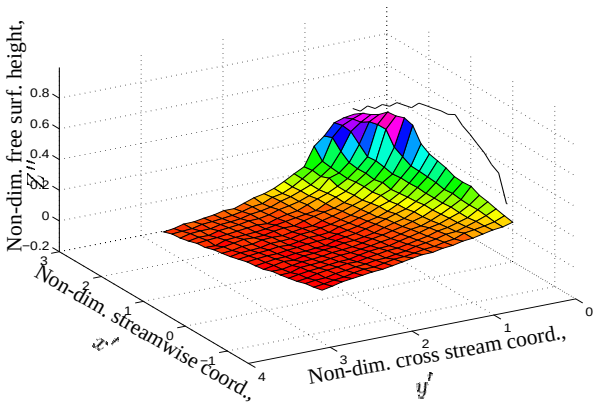

FIGURE 12: Non-dimensional water surface topography along with the contact line from a larger scale experiment; $\theta = 13.4°$, $\phi = 0°$, $U = 2.43m/s$, $d = 7.56cm$, and $\mathbf{F} = 2.81$. The leading edge of the deflecting plate is located at $(x', y') = (0, 0)$.

wave. Also shown is the contact line which defines the location of the deflecting plate. Since it was necessary to displace the edge of the grid from the deflecting plate by several cm, water surface elevation readings were not taken for a narrow strip between the grid edge and the deflecting plate. These missing data account for the apparent discontinuity in Figure 12 between the water surface topography and the contact line. Another example of a water surface topography from the larger scale experiments for $\theta = 26.6°$ is shown in Figure 13 with the corresponding contact line. Comparison of these two figures shows that an increase in θ leads to an increase in amplitude of the breaking wave. Other water surface topographies for a given θ did not show significant change over the narrow range of $\mathbf{F}$ tested in the larger scale experiments.

CONCLUSIONS

The formation of a bow wave on a ship was simulated in the laboratory as a part of a program to examine the air entrainment by breaking bow waves. Flow visualization experiments were used to identify the main features of the flow which may be helpful in characterizing the air entrainment process. Experiments using an electronic point gage were conducted to study changes in the bow wave contact line and the three-dimensional shape of the early region of the bow wave for different

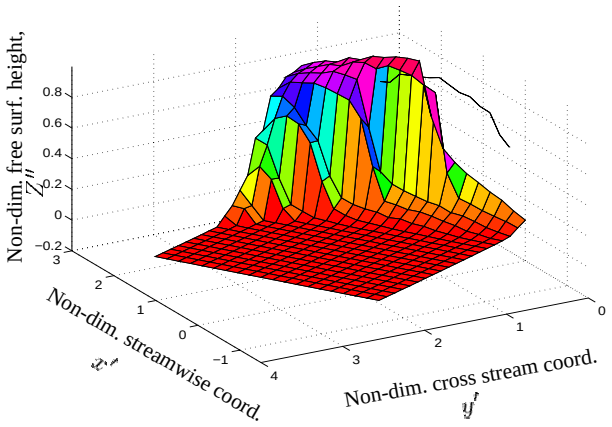

FIGURE 13: Non-dimensional water surface topography along with the contact line from a larger scale experiment; $\theta = 26.6°$, $\phi = 0°$, $U = 2.39m/s$, $d = 7.56cm$, AND $\mathbf{F} = 2.77$. The leading edge of the deflecting plate is located at $(x', y') = (0, 0)$.

deflection angles and flow parameters. The normalized amplitude of the bow wave contact line was shown to increase with increasing angle θ and $\mathbf{F}$. Comparison of our smaller scale experiments to Ogilvie's [1969] data showed that similar results can be produced by experiments using either a towed wedge of limited draft in a larger depth or by using a deflector plate extending the full depth in a supercritical free surface flow.

ACKNOWLEDGEMENTS

The authors wish to acknowledge Caltech students Don Kwak, Bruce Nairn, Janet Sun, and Sudipto Sur for their help in conducting the experments. They are also grateful for the support of the Office of Naval Research under grant number N00014-94-1-1210.

REFERENCES

Bonetto, F. and Lahey, R.T., "An Experimental Study on Air Carry Under Due to a Plunging Liquid Jet", Journal of Multiphase Flow, 19, 1993, 281-294.

Chanson, H. and Cummings, P.D., "Modeling Air Entrainment in Plunging Breakers", International Symposium on Waves–Physical–Numerical Modeling, Vancouver 1994.

Cipriano, R.J. and Blanchard, D.C., "Bubble and Aerosol Spectra Produced by a Laboratory Breaking Wave", Journal of Geophysical Research, 86, 1981, 8085-8092.

Duncan, J.H., "An Experimental Investigation of Breaking Waves Produced by a Towed Hydrofoil", Proc. R. Soc. London, A377, 1981, 331-348.

Lamarre, E. and Melville, W.K., "Air Entrainment and Dissipation in Breaking Waves", Nature, 351, 1991, 469-472.

Loewen, M.R., M.A. O'Dor, and M.G. Skafel, "Bubbles Entrained by Mechanically Generated Breaking Waves", Journal of Geophysical Research, 101, 1996, 20759-20769.

Miyata, H. and Inui, T., "Non-linear Ship Waves", Advances in Applied Mechanics, 24, 1984, 215-288.

Ogilvie, F.T., "The Wave Generated by a Fine Ship Bow", 9th Symposium on Naval Hydrodynamics, Paris 1969, 1483-1524.

Vanoni, V.A., N.H. Brooks, and F. Raichlen, "40m precision tilting flume", W.M. Keck Laboratory of Hydraulics and Water Resources, California Institute of Technology, Technical Memo. 67-3, October, 1967.